Turbulence and mixing around a submerged obstacle subject to regular waves

by

A. Balzano[(1)], B. Dessì[(2)], and G. Querzoli[(3)]

Università di Cagliari, Dipartimento di Ingegneria del Territorio

Piazza d'Armi, 16, 09123 Cagliari, Italy

[(1)]E-mail: balzano@unica.it

[(3)]E-mail: querzoli@unica.it

ABSTRACT

An experimental investigation of the velocity field generated in the vicinity of a rectangular, submerged obstacle by regular incident wave trains was carried out in a flume. Velocity measurements were carried out by means of Particle Tracking Velocimetry, whereas wave elevations at four locations were measured by resistive probes. The wave motion has been analysed in terms of spatial distribution of phase averaged velocity, vorticity, turbulent kinetic energy and turbulent kinetic energy production, and of total kinetic energy. Reflection coefficient were then computed after decomposition of the incident and reflected wave components with the method of Goda and Suzuki (1976).

As shown in Fig. 1, the velocity field around the obstacle is characterised by the formation of vortices at the two upper corners, of increasing magnitude and tendency to detachment with increasing relative wave length. Detail analysis of the space distributions of vorticity, turbulent kinetic energy and turbulent kinetic energy production at different phases enables recognising the maxima of turbulent kinetic energy production and the transport of fully developed vortices by the mean motion as occurring in different instants. Two time maxima of turbulent kinetic energy production are observed at both sides of the obstacle, occurring at times differing by about half the wave period, with one of the two being noticeably larger on the lee side and two more or less equal on the weather side. Moreover, it is shown that while on the lee side of the obstacle the total turbulent kinetic energy is larger than on the weather side, a larger production of turbulent kinetic energy occurs at the weather side. This confirms that nonlinear modes – which, according to literature, are found only on the lee side – are in fact originated in the weather side of the obstacle and transported downstream.

The reflection coefficient, defined as the square root of the ratio of the seaward and landward directed wave components measured seaward of the obstacle position, decreases ranging from high frequencies (short waves, high relative depth, *d/L*) to low frequencies (long waves, small relative depth) both in the absence and in the presence of the obstacle. The behaviour in the presence of the obstacle is consistent with the fact that energy dissipation is a maximum for the longest waves and occurs over the obstacle. The latter circumstance can be an explanation of the behaviour without the obstacle, since the measurement station was located relatively far from the downstream end of the channel.

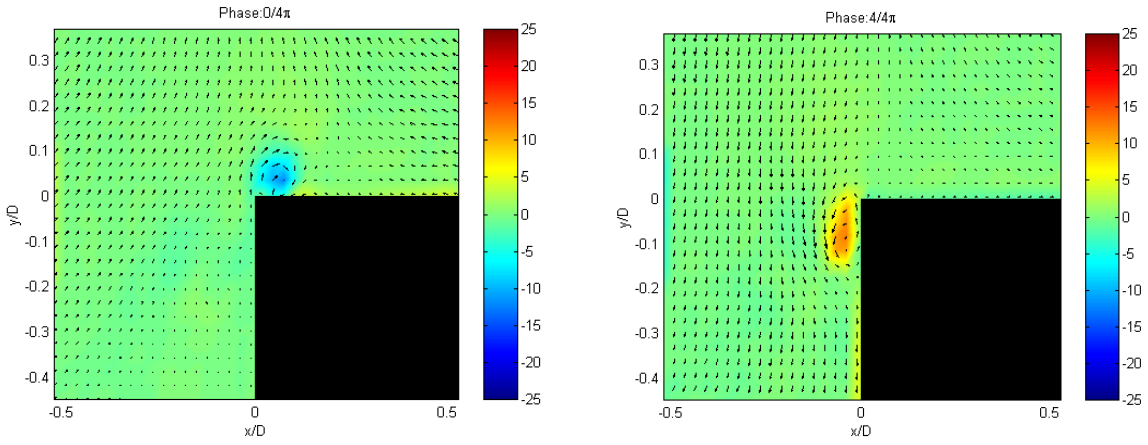

Fig. 1. Distribution of velocity (vectors) and vorticity (colour map) at two phases under a 1 s period wave, at the lee side of the obstacle.

1. INTRODUCTION

Designing longshore detached breakwaters for littoral protection requires estimating the wave motion transformation induced by the structure, on both its lee and seaward sides. This is necessary to assess the static equilibrium conditions of the breakwater and to predict the morphologic evolution of the shoreline and water quality conditions in the sheltered area. In the last years submerged or nearly emerging breakwaters are being seen with increasing favour, due to their reduced environmental and, more specifically, visual impact.

One of the most peculiar features of the hydrodynamic field which is induced by these structures is related to the propagation of the incident wave on quite small water depths over the top of the breakwater, resulting in non-linear components being generated (Grue, 1992; Driscoll et al., 1992; Beji and Battjes, 1993; Ohyama and Nadaoka, 1994). In particular, Grue (1992) showed that free modes, which are located in the lee side of the obstacle only, are larger than forced modes, and dissipations increase with increasing harmonics' amplitude. The effects of the presence of such a structure can be divided in two main categories: the first includes large scale effects, i.e. the modification of the flow and wave pattern, that are observable on a length scale of the same order as the breakwater length, and affect mainly the currents in the proximity of the shore and the beach morphology; the second category includes the local effects, whose length scale is of the order of the breakwater height, such as turbulence and vortex generation.

The study presented here focuses on the second kind of phenomena, with the aim to understand the mechanism involved in the non-linear transformation of waves, vortex generation and mixing around the obstacle. These are the fundamental elements to comprehend the physical mechanism underlying wave dissipation and reflection by the breakwater and mass transfer between weather and lee side. The dissipation of the wave energy is a measure of the effectiveness of the structure, whereas mixing between the sides of the breakwater is important for the breakwaters that are long enough to constitute a significant barrier to refreshment of waters in the proximity of the coastline.

In order to minimise the parameters controlling the phenomenon, a simple, but representative, experiment was performed: a rectangular obstacle was placed in a glass water channel equipped with a wavemaker generating regular waves. The flow field around the rectangular obstacle was investigated by means of the Particle Tracking Velocimetry. The technique allowed for the recognition of particle trajectories, hence the phase averaged Eulerian velocity fields and its statistics were evaluated.

2. EXPERIMENTAL SET-UP AND MEASURING TECHNIQUE

The experimental tests were carried out in a 21 m long laboratory flume with a wave-maker of the piston type installed (Fig. 2). The still water cross section was equal to 31 × 40 cm, and the obstacle was a parallelepiped of dimensions 40 × 31 × 20 cm (l×w×h). On the side opposite to the piston of the wave-maker, an absorber was placed in order to minimise the wave energy impinging on the obstacle from the lee side. The absorber was constituted of a narrow, oblique stratification of iron net located in the last couple of meters of the channel. Four resistive probes were placed between the wave-maker and the obstacle to measure the time history of the water elevation. On the basis of the measurements of these probes, the decomposition of incident and reflected wave spectra was carried out with the method by Goda and Suzuki (1976) in order to evaluate the reflection coefficients in the experimental conditions. Distance between probes, Δx, was arranged so as to obtain values of the ratio $\Delta x/L$, with L being the wave length, as far as possible from the critical value, 0.5, for all four period considered.

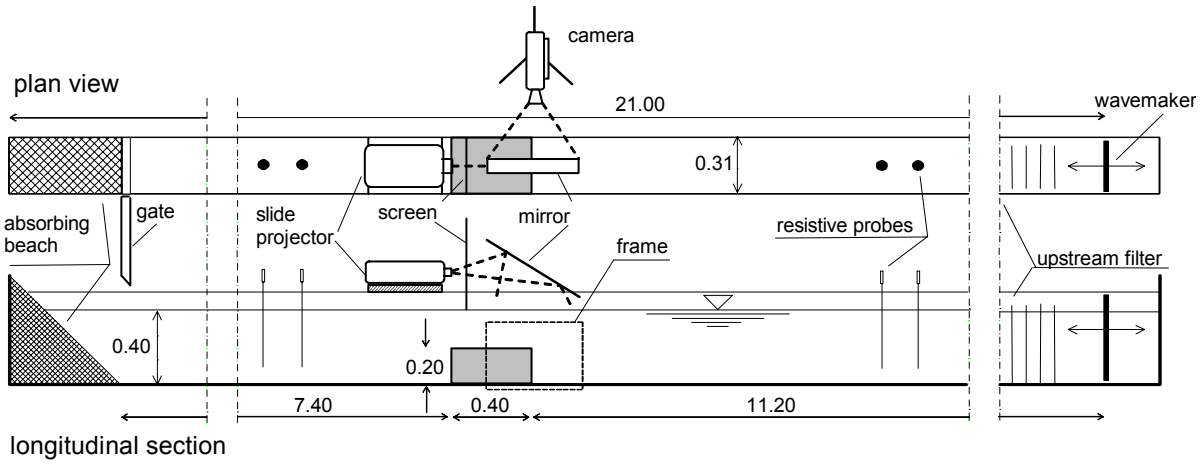

Fig. 2. Experimental equipment (measures in m).

The working fluid was seeded with small non-buoyant particles, about 100μm in diameter. The investigation area was illuminated with a light sheet generated by a slide projector, and images were recorded by a 3-CCD, DV camera, orthogonal to the light sheet. Frame sequences were then digitised at the frequency of 25 per second. Each frame was decomposed into its constituent fields and analysed in order to reach a sampling rate of 50 Hz. Particle Tracking Velocimetry analysis consists of three main steps: particle identification, trajectory recognition and velocity evaluation.

Particle identification was based on thresholding images and recognising particles as connected sets of bright pixels. As a matter of fact, before thresholding, a background subtraction was performed on the image. Background at a given location was computed as the average of the grey levels in a square neighbourhood centred on the considered pixel. The main effect of the background removal is to account for the variation of the pedestal level over the image, due to the non-uniform illumination of the investigated area. Nevertheless, assuming that the size of the averaging area is comparable to the radius of the particle images (in the present analysis it was about 3 times larger), the subtraction of the local background has the side-effect to enhance the particle recognition by reducing the noise at the border of the particles and by separating partially overlapping particles. The reason for this behaviour is that the background is overestimated in the neighbourhood of each grey-level peak. As a consequence when it is subtracted from the image it tends to darken every bright zone around peaks. This is clearly seen in the one-dimensional examples shown in Fig. 2.

On the left plot the procedure is applied to a particle with some noise at its border (i.e. the small peak on the right). Before processing a low threshold (about 100) could lead to the identification of two particles, one for the main peak and one for the secondary peak; after processing only one well identified peak exceeds the zero grey level. The plot on the right of the same figure shows the case of two partially overlapping particles: also in this case, before processing, a low threshold (below 120) would lead to the identification of a single spot, whereas after processing two separate particles would be recognised for each positive level of the threshold.

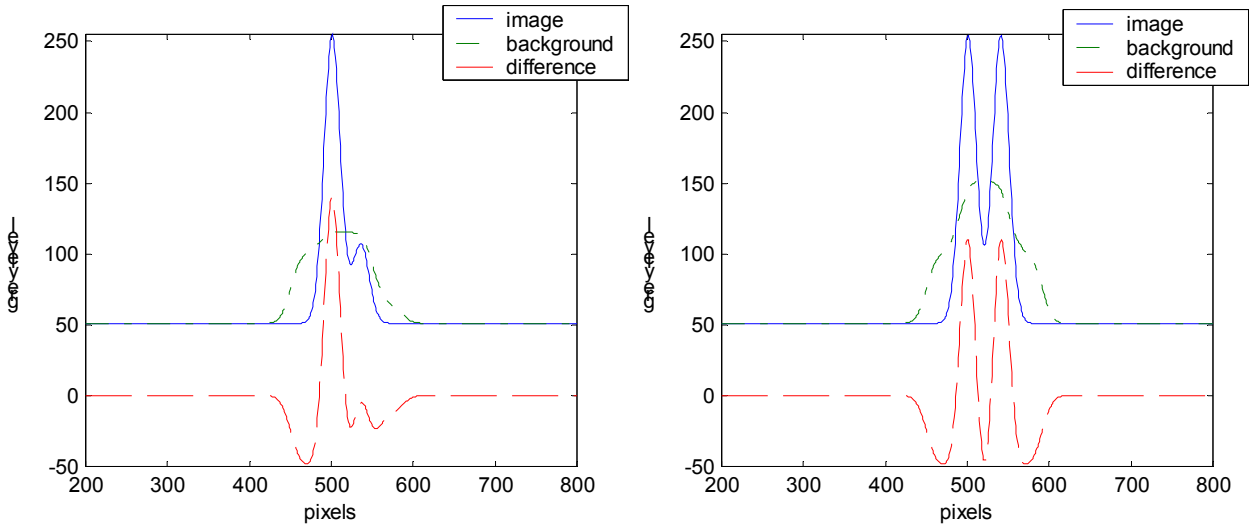

Fig. 3. One-dimensional examples of side-effect of background subtraction: noise removal(left) and particle separation (right).

Trajectories were recognised evaluating the position of particles on subsequent frames on the basis of two limiting criteria: maximum distance between particles (i.e. maximum velocity) and maximum difference between successive particle displacements (i.e. maximum acceleration). Moreover, when more than one particle satisfied the latter criterion, the one corresponding to the minimum acceleration was chosen. Though this criterion is not completely physically justified, it was observed that, in practise, it was effective since wrong trajectories are more likely characterised by uncorrelated, sudden changes in direction and displacement magnitude and therefore by high accelerations. An example of the acquired trajectories is shown in Fig. 4.

From the particle trajectories, velocity fields were evaluated trivially by dividing the particle displacements by the time interval between frames. Experiments were carried out in five different conditions whose main parameters are listed in Table 1. Each run was repeated three times with the same parameters: first to determine wave elevations without the obstacle, then to measure elevations in presence of the obstacle, and finally to measure velocity fields.

It is to be noted that the Reynolds number used here is different from those proposed by Ohyama and Nadaoka (1994) and Huang and Dong (1999). Indeed, while it seems incorrect assuming the shallow water wave celerity as the velocity scale, as the former authors did, even the need for a definition resulting in increasing Reynolds numbers with increasing

vortex generation and energy dissipation is not as obvious as pretended by the latter authors. Indeed, it should be kept in mind that, in principle, due to the sharp corners and related singularities of the wall profile, separation would occur whatever the Reynolds number. Moreover, not all the runs considered by Huang and Dong (1999) are characterised by shallow water conditions, as supposed in the derivation of the velocity scale. Finally, assuming the velocity scale to be $H\,L/\,T\,d$ leads to the contradictory conclusion that the time scale is not the wave period, whatever the characteristic length assumed. On the other hand, the behaviour of the Keulegan-Carpenter number as defined by Ting and Kim (1994) and Huang and Dong (1999) is consistent with its meaning of maximum particle displacement to obstacle length ratio.

Table 1 - Parameters of experimental runs (d is water depth and ν *is water kinematic viscosity).*

	run #1	run #2	run #3	run #4
Incident wave height H_i (cm)	2.99	2.89	3.29	3.16
Incident wave length L (m)	0.56	0.78	1.06	1.46
Incident wave period T (s)	0.60	0.71	0.83	1.00
Ursell number $N_u = (H_i\,L^2)/d^3$	0.148	0.279	0.575	1.059
Keulegan-Carpenter number $N_{kc} = (H_i\,L)/d^2$	0.105	0.142	0.218	0.289
Reynolds number $N_{Re} = (H_i\,d)/(T\,\nu)$	19932	16303	15865	12647

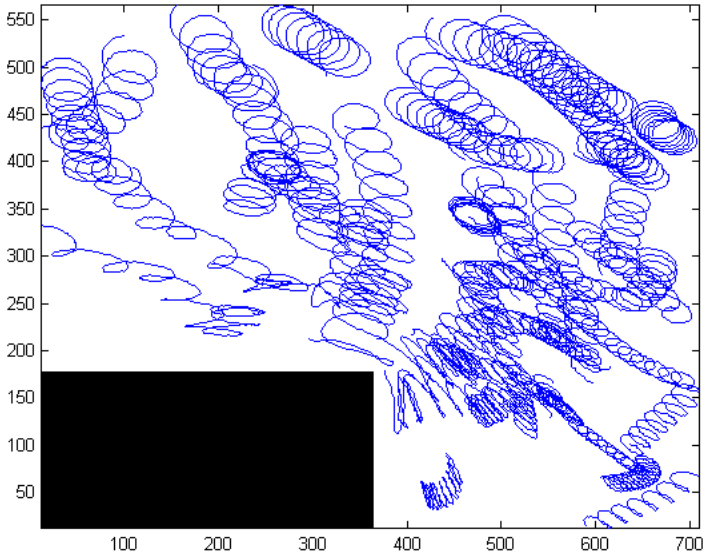

Fig. 4. Trajectories acquired around the weather-side corner of the submerged obstacle (unit is pixel).

3. EXPERIMENTAL RESULTS

Velocity samples obtained by PTV were used to compute phase averaged statistics on a regular grid, namely velocity mean values and variances. The former represents the coherent part of the field, that is repeated during each period; the latter how much the phenomenon is repeatable in the different zones of the field. During the wave period, in the proximity of the upper corners of the obstacle, a vortex is generated alternatively on the horizontal and vertical wall, which dimensions and tendency to detachment increase for increasing wave length, that is, for decreasing relative depths, d/L. This behaviour is clearly observed in Figs. 5 and 6, that represent the mean velocity and vorticity distributions at the lee- and weather-side corners for eight phases of run #4. In particular, at phases 0 and π the vortex is completely formed, whereas at phases π/2 and 3/2π there is a production of vorticity distributed over the obstacle walls due to shear. Phase zero has been defined for each side of the obstacle as the one at which velocities above the corresponding corner have vertical upward direction, that is, according to linear theory, when the free surface is in its hydrostatic position. Vorticity is made dimensionless by means of the incident wave period, T.

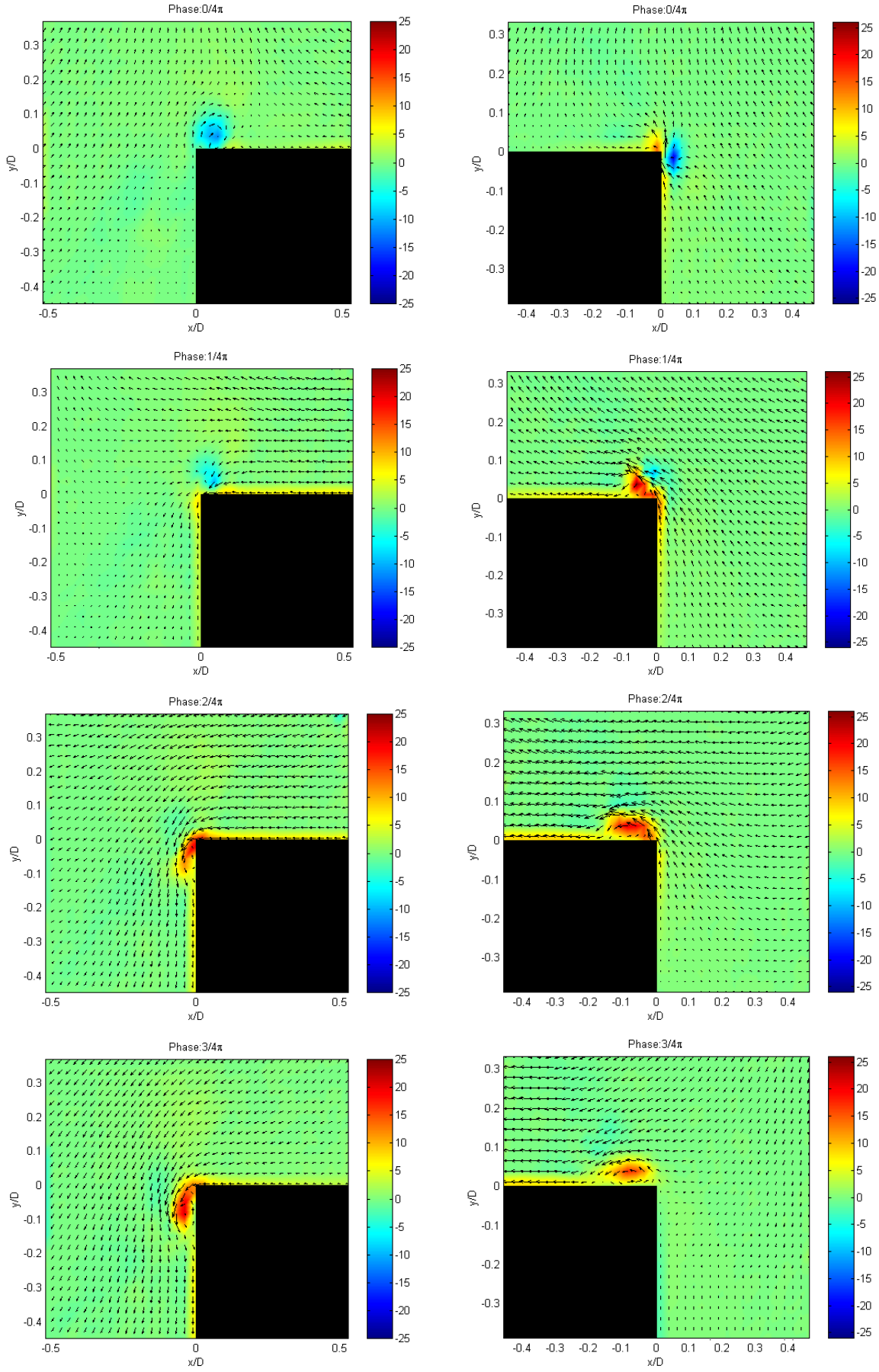

Fig. 5. Phase averaged mean velocity (vectors) and vorticity (colour map) for run #4. From top to bottom phases $\Phi = 0, \pi/4, \pi/2, 3/4\pi$. Lee side on the left, weather side on the right.

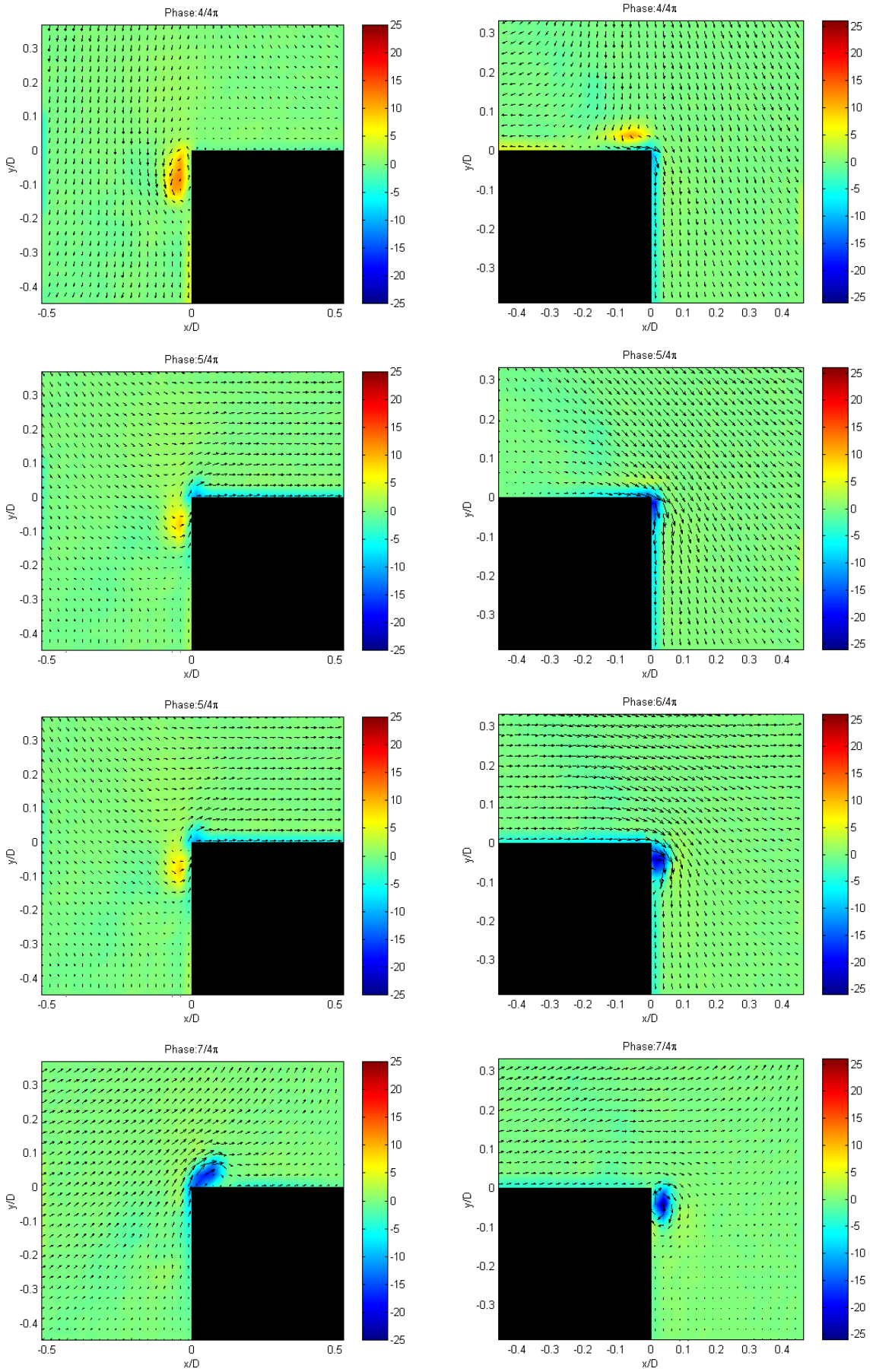

Fig. 6. Phase averaged mean velocity (vectors) and vorticity (colour map) for run #4. From top to bottom phases $\Phi = \pi, 5/4\pi, 3/2\pi, 7/4\pi$. Lee side on the left, weather side on the right.

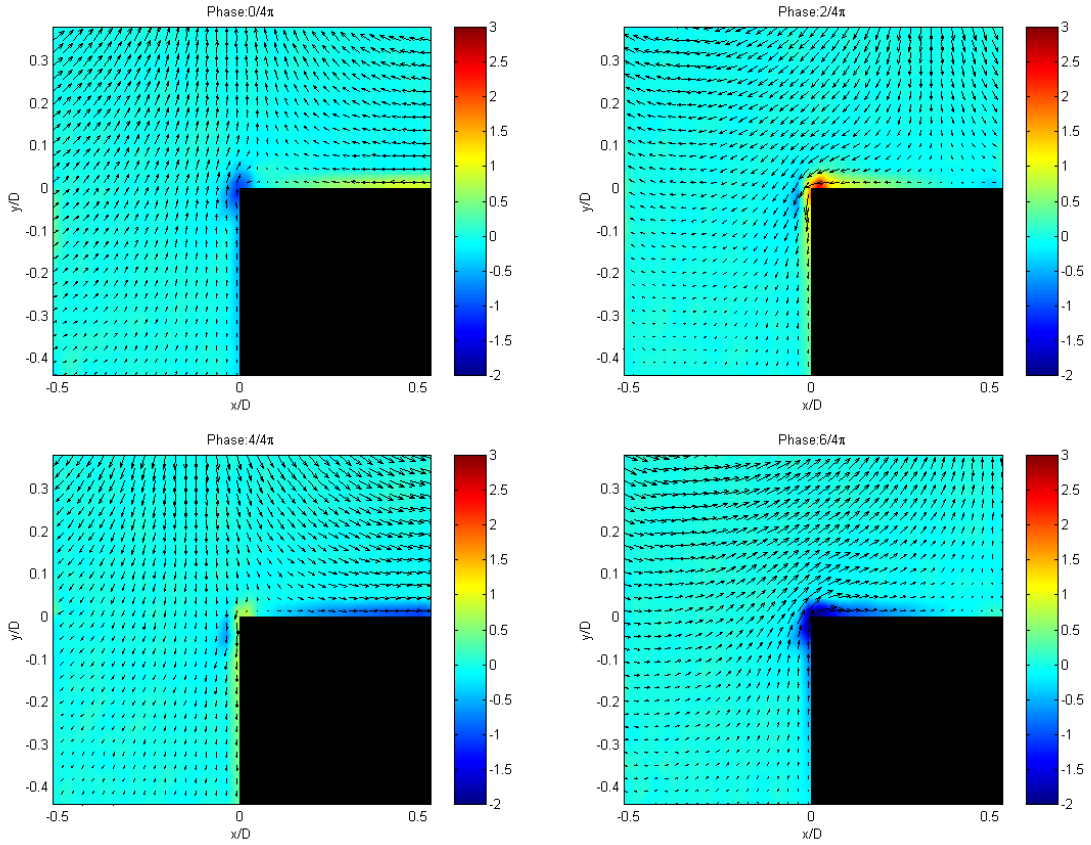

Fig. 7. Phase averaged mean velocity (vectors) and vorticity (colour map) at the lee side for run #1. From top left to bottom right phases $\Phi = 0, \pi/2, \pi, 3/2\pi$.

The generation of the vortex is due to the strong tangential velocity at the obstacle wall, oriented towards the corner ($\Phi = \pi/2,\ 3/2\pi$). The high velocity at the wall determines detachment at the corner, from which a jet-like flow originates. At the beginning, this flow causes only turbulence; later, the motion begins to organise in a vortex, that is completely formed after about a quarter of period. Vorticity is then transported by the flow, its residuals being still visible as the next counterturning vortex develops.

In Fig. 7 the same quantities are shown for four phases of run #1, corresponding to the least wave period. Although larger values of vorticity are still found in the neighbourhoods of the corners, vortices of sizes comparable to the ones for run #4 are not seen.

The presence of turbulence, in addition to the presence of the vortex, can be observed in Fig. 8, that shows the phase averaged turbulent kinetic energy: $\varepsilon = \overline{u'^2} + \overline{v'^2}$, made dimensionless by the square of the velocity scale, $U = H_i / T$. This energy is transferred from the mean motion and dissipated by viscosity. Consequently, it is subtracted from the incident wave energy after the incident wave height has been measured, which results in decreasing the value of the measured reflection coefficient of the wave.

The overall perturbation induced to the mean field by the obstacle can be pointed out by analysing the total kinetic energy, $E = \overline{u^2} + \overline{v^2}$. In Fig. 9, the mean kinetic energy around the top corners of the obstacle is shown for runs #1 and #4. In the case of undisturbed wave field it should be horizontally uniform, and decreasing with increasing depths. However, the waves generated in run #4 induce large velocities even in the proximity of the obstacle since the wave-length is large compared to the water depth. As a consequence, the vortex is intense and its energy predominates on any other motion. Close to the corner there is a sharp peak, corresponding to the zone visited by the vortex. Moreover, the obstacle determines a perturbation that corresponds to an increase of the kinetic energy above the corner, particularly in the presence of a well-formed circulation cell. Conversely, the short waves generated during run #1 induce lower velocities at the depth of the obstacle top. As a consequence, the energy of the waves close to the surface is dominant and the presence of the obstacle does not perturb the field too much. These different behaviours are only in partial agreement with the evaluation of the reflection coefficients obtained from free surface measurements (Table 2). Note that these reflection coefficients include not only physical reflection on the obstacle's weather side: since they are deduced on the basis of the spectra of rightward and leftward travelling components measured on the seaward side, they

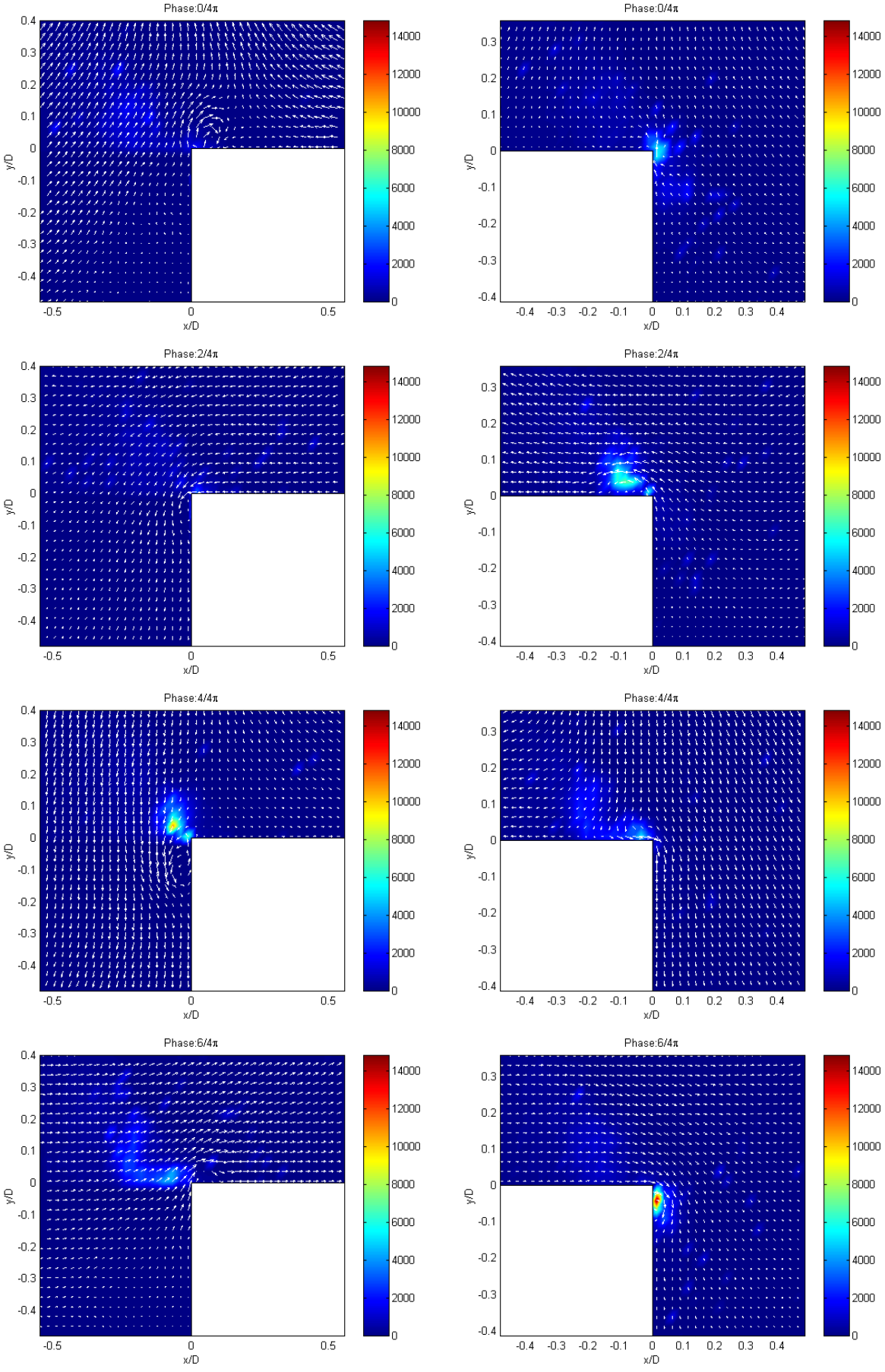

Fig. 8. Phase averaged turbulent kinetic energy (colour map) with velocity field superimposed for run #4. From top left to bottom right phases $\Phi = 0,\ \pi/2,\ \pi,\ 3/2\pi$.

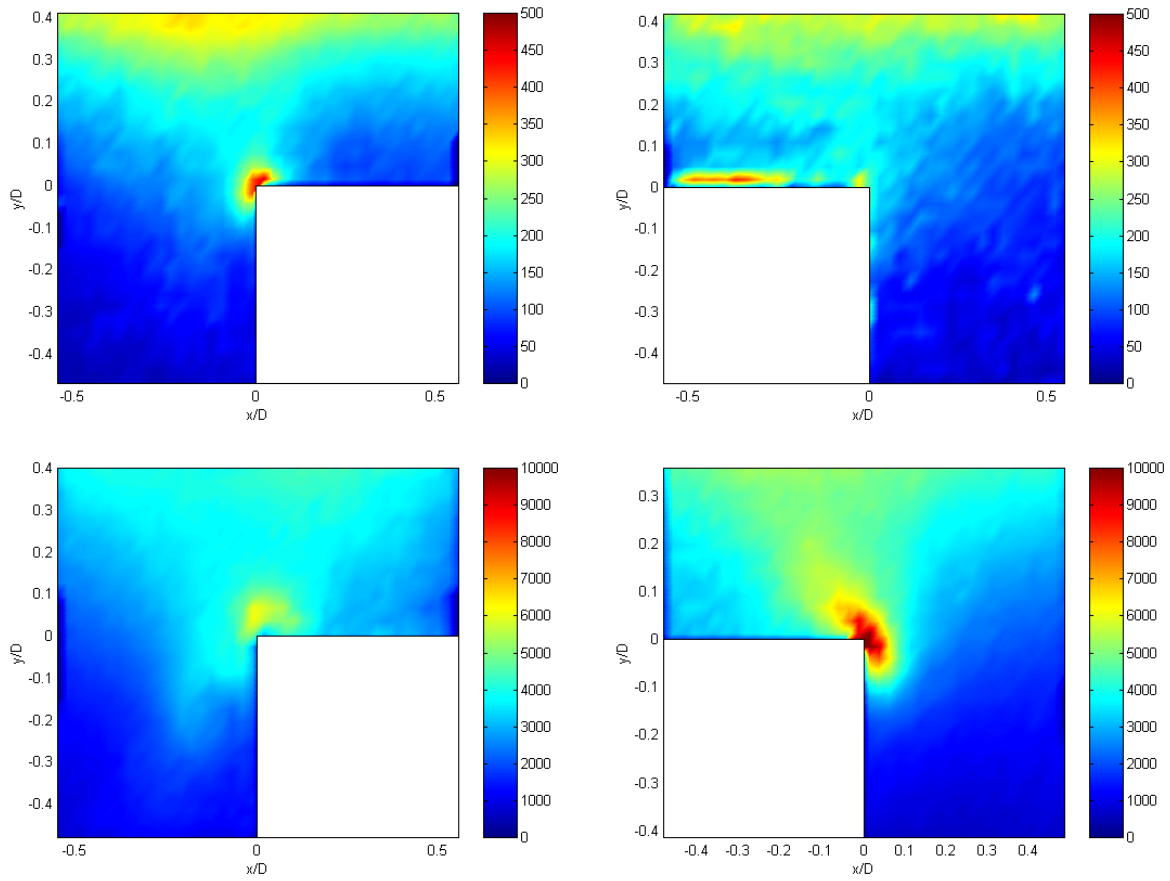

Fig. 9. Mean kinetic energy for runs #1 (top) and #4 (bottom) .

Table 2 – Reflection coefficients with (k_r) and without (k_{r0}) the obstacle and their ratio.

	run #1	run #2	run #3	run #4
k_r	0,15	0,097	0,058	0,037
k_{r0}	0,18	0,070	0,061	0,060
k_r / k_{r0}	0.83	1.39	0.95	0.62

do include also the effects of transmission, dissipation and reflection at the end of the channel of the incident wave, and again dissipation and transmission over the obstacle in the seaward travel.

As a matter of fact, the reflection coefficients decrease with increasing wave period both in the presence and in the absence of the obstacle. However, the ratio of the two has a maximum for run #2, corresponding to amplification of the reflected component, and smaller values at the two extremes of the period range. The above discussion, instead, would suggest a decreasing ratio with increasing wave period due to the increasing effects of viscous dissipation and separation related to the strong oscillating vortex. It is also to be noted that it is not possible comparing these values of the reflection coefficients with those obtained by other authors (Grue, 1992; Ting and Kim, 1994). Indeed, the detailed studies by the authors mentioned above are more concerned with the evaluation of high order harmonics, with the value $k_r = 0.2$ reported by Grue (1992) being related to a very high value of the obstacle height to water depth ratio, much larger than the one used in the present study, and similar values given by Ting and Kim (1994) result from linear theory. This fact suggests that in that range of periods the velocity field is someway resonant; nevertheless the further investigation needed for an exhaustive interpretation is planned for the near future.

To get further insight in the dynamics of turbulence, the rate of turbulent kinetic energy production has been analysed, defined as the source term in the equation of turbulent kinetic energy balance, here written in tensor form (Hinze, 1959):

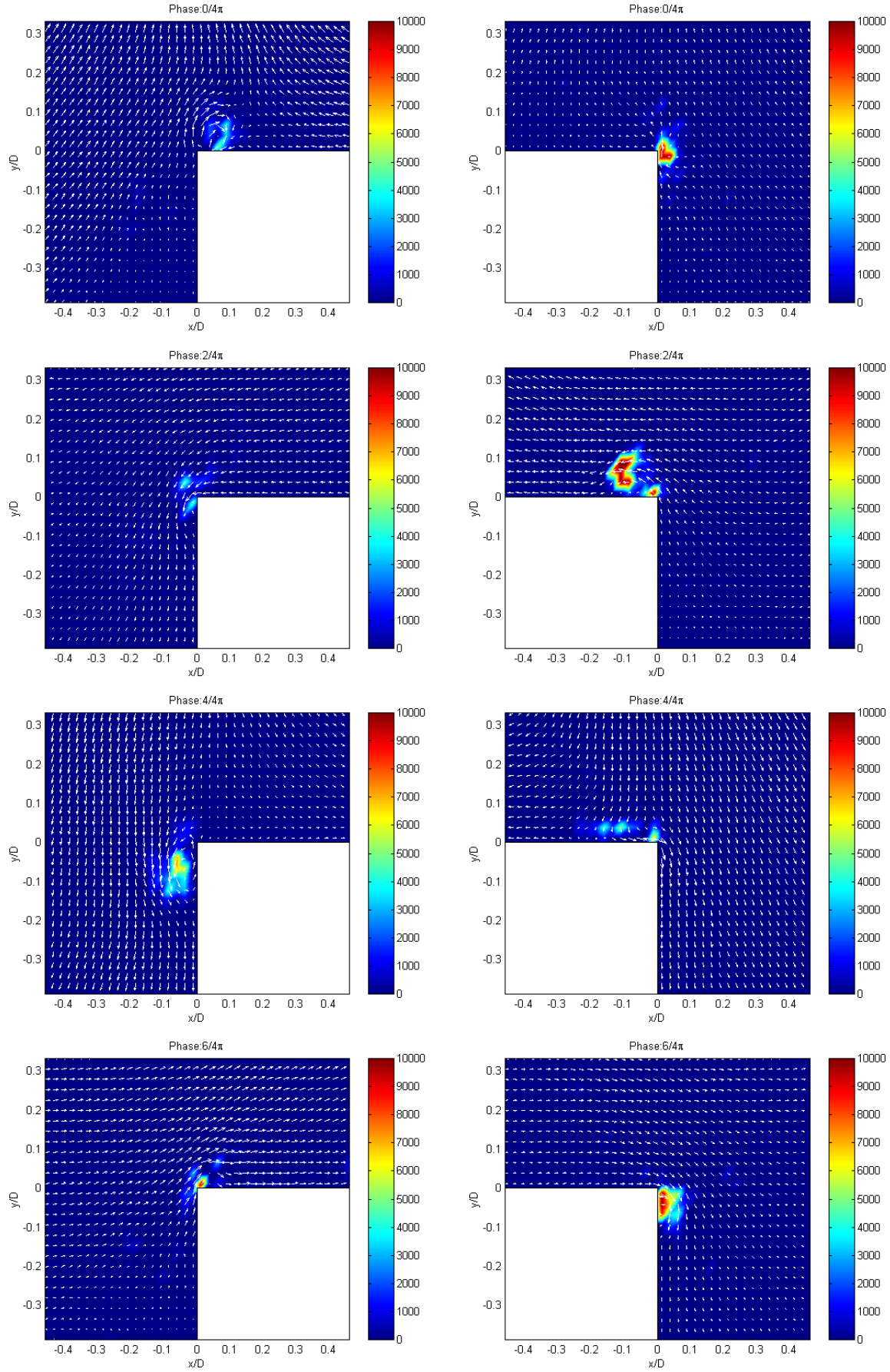

Fig. 10. Phase averaged rates of turbulent kinetic energy production with velocity field superimposed for run #4. From top left to bottom right phases $\Phi = 0, \pi/2, \pi, 3/2\pi$.

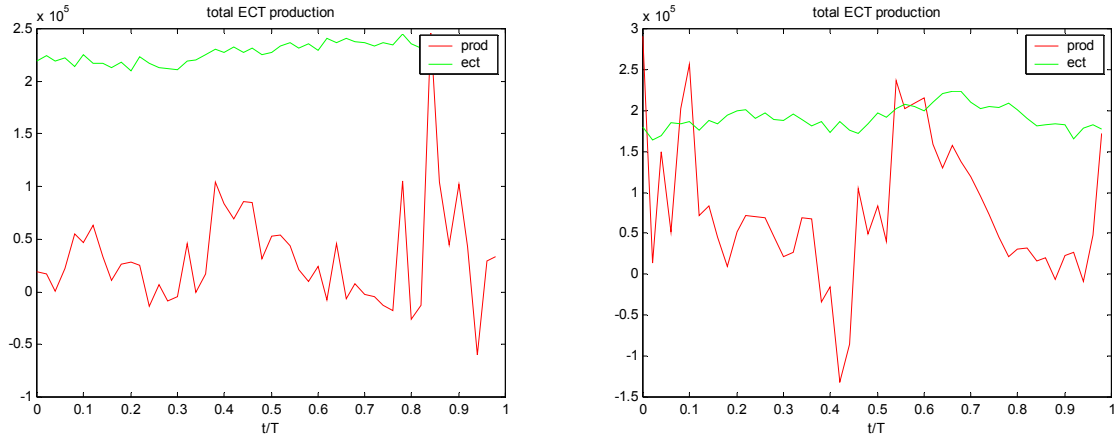

Fig. 11. Turbulent kinetic energy (green line) and rate of turbulent kinetic energy production (red line) integrated over the whole measurement fields as a function of time. Lee side on the left, weather side on the right.

$$-\overline{u'_i\, u'_j}\,\frac{\partial \overline{u}_j}{\partial x_i} \tag{1}$$

with the primes denoting fluctuating velocity components, the overbar the phase-averaging operator, and summation on both indices, *i* and *j*, is intended . Distributions of phase averaged rates of turbulent kinetic energy production are shown in Fig. 10 for four phases of run #4.

The above analysis substantially confirms the relevance of the top corners of the obstacle in mechanism of generation turbulent kinetic energy. It is also to be noted that at phases 0 and π the vortices on the lee side are well formed and transported by the mean motion, while the rate of production of turbulent energy are negligible. A similar situation is observed on the weather side, although the fully formed vortices' phase are not shown in Fig. 10.

A detail of the temporal evolution of both turbulent kinetic energy and relevant production rate integrated over the whole measurement fields is given in Fig. 11. In agreement with Fig. 10, the rate of production of turbulent kinetic energy has two peaks occurring at opposite phases, during the vortices' generation. On the weather side the peaks have nearly equal magnitude, whereas on the lee side the one corresponding to the vortex generation on the top surface of the obstacle is more intense.

In addition, it is interesting to note that while the higher levels of turbulent kinetic energy are found in the lee side of the obstacle, the higher production rates are found on the weather side. This is in agreement with the mechanism of formation of free nonlinear modes described by other authors (Grue, 1992; Driscoll et al., 1992; Beji and Battjes, 1993; Ohyama and Nadaoka, 1994, Huang and Dong, 1999).

4. CONCLUSIONS

Particle Tracking Velocimetry together with traditional measurement techniques based on resistive probes have been applied to the study of the propagation of monochromatic waves over a submerged obstacle in a laboratory channel.

Joint analysis of velocity fields and free surface measurements made it possible pointing out the different behaviours of waves of different periods and heights in the above experimental conditions. The reflection coefficient, defined as the square root of the ratio of the seaward and landward directed wave components measured seaward of the obstacle position, decreases ranging from high frequencies (short waves, high relative depth, *d/L*) to low frequencies (long waves, small relative depth) both in the absence and in the presence of the obstacle.

Actually, the presence of the obstacle resulted in decreasing reflection coefficients, as defined above, for waves of larger period, for which intense generation of vorticity and boundary layer separation are effective in increasing energy dissipation, occurring mainly over the obstacle. This is in agreement with the mechanism described in the literature. The behaviour of the reflection coefficient in the absence of the obstacle could be ascribed to the relative long distance between the downstream end of the channel and the measurement station. Indeed, although higher reflection of longer waves is expected at the downstream end, actually the higher losses also related to smaller relative depths could make

the value of the seaward travelling component of longer waves at the measurement station smaller than that of shorter ones. The ratio of the reflection coefficients measured in the presence and in the absence of the obstacle have a maximum, larger than one, for an intermediate frequency, while for the higher frequency the ratio is less than one.

In addition, details of the space distributions of vorticity, turbulent kinetic energy and turbulent kinetic energy production at different phases have been given. This enables recognising the maxima of turbulent kinetic energy production and the transport of fully developed vortices by the mean motion, with negligible production of turbulent kinetic energy, as occurring in different instants. Two maxima of turbulent kinetic energy production are observed, occurring at times differing by about half the wave period, with one of the two noticeably larger on the lee side and two more or less equal on the weather side. Moreover, it is shown that while on the lee side of the obstacle the total turbulent kinetic energy is larger than on the weather side, a larger production of turbulent kinetic energy occurs at the weather side. This confirms that nonlinear modes – which, according to literature, are found only on the lee side – are in fact originated in the weather side of the obstacle and transported downstream.

REFERENCES

Beji, S. e Battjes, J.A.(1992), "Experimental investigation of wave propagation over a bar", *Coastal Engineering, 19.*

Driscoll, A. M., Dalrymple, R. A., Grilli, S.T., (1992), "Harmonic generation and transmission past a submerged rectangular obstacle". *Proc.23 Int. Coastal Engineering Conference,* Venice, ASCE.

Goda, Y. e Suzuki, Y.(1976), "Estimation of incident and reflected wave in random wave experiments", *Proc15 Int. Conference on Coastal Engineering,* Vol. 1, ASCE, New York.

Grue, J.,(1992), "Nonlinear water waves at a submerged obstacle or bottom topography". *J. Fluid Mech. 244.*

Hinze, J.O. (1959), *"*Turbulence*". McGraw Hill.*

Huang, J.H., Dong, C.M., (1999), "Wave deformation and vortex generation in water waves propagating over a submerged dike". *Coastal Engineering, 37.*

Ohyama, T., Nadaoka, K.,(1994), "Transformation of a nonlinear wave train passing over a submerged shelf without breaking". *Coastal Engineering, 24.*

Ting, F.C.K., Kim, Y.K., (1994), "Vortex generation in water waves propagating over a submerged obstacle". *Coastal Engineering, 24.*